Shear-induced contact area anisotropy explained by a fracture mechanics model

A. Papangelo, J. Scheibert, R. Sahli, G. Pallares, M. Ciavarella

Shear-induced contact area anisotropy explained by a fracture mechanics model

A. Papangelo,[1,2] J. Scheibert,[3] R. Sahli,[3] G. Pallares,[3,4] and M. Ciavarella[1,2]

[1] *Dipartimento di Meccanica, Matematica e Management, Politecnico di Bari, Viale Japigia 182, 70126 Bari, Italy*

[2] *Hamburg University of Technology, Department of Mechanical Engineering, Am Schwarzenberg-Campus 1, 21073 Hamburg, Germany*

[3] *Univ Lyon, Ecole Centrale de Lyon, ENISE, ENTPE, CNRS, Laboratoire de Tribologie et Dynamique des Systèmes LTDS, UMR 5513, F-69134, Ecully, France*

[4] *CESI, LINEACT, Zone Aéroportuaire Méditerranée, 34130 Mauguio, France*

(Dated: June 4, 2019)

This paper gives a theoretical analysis for the fundamental problem of anisotropy induced by shear forces on an adhesive contact, discussing the experimental data of the companion Letter. We present a fracture mechanics model where two phenomenological mode-mixity functions are introduced to describe the weak coupling between modes I and II or I and III, which changes the effective toughness of the interface. The mode-mixity functions have been interpolated using the data of a single experiment and then used to predict the behaviour of the whole set of experimental observations. The model extends an idea by Johnson and Greenwood, i.e. to solve purely mode I problems of adhesion in the presence of a non-axisymmetric Hertzian geometry, to the case of elliptical contacts sheared along their major or minor axis. Equality between the stress intensity factors and their critical values is imposed solely at the major and minor axes. We successfully validate our model against experimental data. The model predicts that the punch geometry will affect both the shape and the overall decay of the sheared contact area.

PACS numbers: 81.40.Pq, 68.35.Np, 62.20.Qp

I. INTRODUCTION

The interplay of adhesion and friction is a problem of fundamental importance in tribology, which ideally should be solved at all scales from tectonic plates to atomic scales (for a recent review of multiscale methods and problems in tribology, see [1]). In the particular case of soft materials, it is already relatively well understood and plays a substantial role in Nature: in many insects, for example, an equivalent of an "adhesive Coulomb friction law" has been described, whereby the normal force to detach the adhesive "pads" is proportional to the shear force simultaneously applied ([2], [3], [4]). For soft materials, a finite contact area is observed also under zero force due to adhesion [5] and as a consequence, friction is measured also under vanishing or even negative normal forces [6][7]. There is no unique framework to study this interaction [8]: for instance for hard materials, although no macroscopic adhesion is found and friction may have a number of origins, Rabinowicz [9][10] attempted to describe friction in terms of surface energy. Another example is the onset of sliding, for which fracture-like surface energy concepts have been used successfully [11],[12],[13].

Here, we consider typically soft materials, for which the first fracture mechanics model and experiment for adhesion and friction interaction was conceived for macroscopic smooth spheres by Savkoor & Briggs [14], who extended the Johnson-Kendall-Roberts (JKR) model [5] to the presence of tangential force. This model however corresponded to a "purely brittle" model where the frictional resistance was neglected and, as such, *greatly underestimated* the interfacial toughness. In that respect, it has been observed that when mode I combines with mode II or/and mode III (see Fig. 1a), the interfacial toughness is greatly increased. The physical explanations for this increase are various (e.g. friction, plasticity, dislocation emission) and cannot be ascribed to a single phenomenon [16]. Since then, a few phenomenological models have been proposed ([17],[18],[19],[20],[21],[22],[23]) which require a Mode-Mixity Function (MMF) $f(\psi)$ [26] to describe the critical condition for propagation

$$G_c = G_{Ic} f(\psi) \tag{1}$$

where G_{Ic} is mode I critical factor (or surface energy, if we assume Griffith's concept), G_c is the critical energy release rate in mixed mode conditions and finally ψ is the "phase angle"

$$\psi_2 = \arctan\left(\frac{K_{II}}{K_I}\right) \tag{2}$$

$$\psi_3 = \arctan\left(\frac{K_{III}}{K_I}\right) \tag{3}$$

being K_{III}, K_{II} and K_I respectively the mode III, mode II and mode I stress intensity factors.

The most recent model in this field is perhaps that by Papangelo & Ciavarella [23] who compared it with recent experimental measurements by Mergel et al. [8], and concluded that the transition to sliding is very sensitive to the choice of the mode-mixity function. Papangelo & Ciavarella's mode-mixity model [23] suggests that upon shearing the contact can experience either a smooth transition from the JKR to the Hertzian contact area or an unstable jump to the Hertzian solution where lighter normal forces favour the latter behaviour. All Linear Elastic Fracture Mechanics (LEFM) models indicate a decay

of the contact area with force, but the overall evolution strongly depends on the effective form of the MMF [23]. Furthermore, the most up to date experimental evidences show that for high normal forces, the decay of the contact area with the tangential force is quadratic [15], while for small normal forces [8] it isn't. Experimental measurements of contact area evolution show that the shape of contact area is circular, according to JKR theory, at zero tangential force and shrinks in an elliptical-like fashion while the shear force is increased ([8], [15], [19]). So far, all LEFM models proposed ([14],[17],[18],[19],[22],[23]) make the approximation to consider the contact as circular, even when sheared. This requires an averaging of the effects of mode II and mode III around the periphery. However, it is well known that sphere/plane contacts loose their initial circularity when submitted to shear, indicating that axisymmetry is a very questionable assumption. Note that recent experimental investigations for rough interfaces composed of many asperities [15] have showed similar anisotropic real area reduction and morphology changes, as discussed extensively in the companion Letter [24]. A better understanding of the simpler sphere/plane contacts is crucial to comprehend shear induced-anisotropy in rough contacts.

In the present paper, we shall extend the axisymmetric theory to include the case of elliptical shrinking of single contact area with the shear force, starting from either circular or even already elliptical contact area. Initial ellipticity typically occurs in the case of rough contacts, where most summits are mildly elliptical, the most common ratio of principal summit curvatures being near 2:1 [25].

The only assumption we make for simplicity is that either the major or the minor axis of the contact ellipse is aligned with the shear force: results will show a sufficiently clear overall picture. In the first part of the manuscript the theoretical model will be introduced, while in the second part it will be validated against the experimental results provided in the companion Letter [24] and in Sahli et al. [15].

II. THE APPROXIMATE JKR THEORY FOR ELLIPTICAL CONTACTS

In absence of tangential force, Johnson and Greenwood [27] (JG in the following) developed an approximate JKR theory for adhesion of an Hertzian profile with differing principal radii of curvature. The contact problem is solved "approximately" in a sense that the equality of the Stress Intensity Factor (SIF) to its critical value K_{Ic} round the periphery is only satisfied at the major and minor axis of the contact ellipse. JG assume a pressure distribution equal to

$$p(x,y) = \frac{p_1 - \alpha x^2 - \beta y^2}{\sqrt{1-(x/a)^2-(y/b)^2}} \tag{4}$$

where a and b are respectively the major and minor semi-axes of the ellipse, (p_1, α, β) are constants to be found and $p(x,y)$ is taken positive (negative) when compressive (tensile). The stress intensity factors at the major and minor axis (respectively a and b) are

$$K_I(a) = \left(\alpha a^2 - p_1\right)\sqrt{\pi a} = K_{Ic} \tag{5}$$

$$K_I(b) = \left(\beta b^2 - p_1\right)\sqrt{\pi b} = K_{Ic} \tag{6}$$

JG impose the SIF at the major and minor axis to be equal to its critical value which, by standard LEFM arguments, is $K_{Ic} = \sqrt{2E^* G_{Ic}}$, where E^* is the plane strain composite modulus of the interface, and G_{Ic} the mode I "toughness" or surface energy. Galin's [28] theorem establishes that any pressure distribution of the form (4) produces a field of quadratic displacements

$$w = w_{00} - w_{20}x^2 - w_{02}y^2 \tag{7}$$

where w_{00} is the indentation and (w_{20}, w_{02}) are constants to be found. Kalker [29] reveals the relation between the sets of constants (α, β) and (w_{20}, w_{02})

$$\begin{bmatrix} w_{20} \\ w_{02} \end{bmatrix} = \left(\frac{b}{E^*}\right)\begin{bmatrix} (\boldsymbol{D}+\boldsymbol{C})\alpha - (b/a)^2\boldsymbol{C}\beta \\ -\boldsymbol{C}\alpha + \left\{\boldsymbol{B} + (b/a)^2\boldsymbol{C}\right\}\beta \end{bmatrix} = \begin{bmatrix} 1/2R_1 \\ 1/2R_2 \end{bmatrix} \tag{8}$$

where $\boldsymbol{K}(e), \boldsymbol{E}(e), \boldsymbol{B}(e), \boldsymbol{C}(e), \boldsymbol{D}(e)$ are complete elliptic integrals of argument $e^2 = 1 - g^2$ $(g = b/a < 1)$ with $e^2\boldsymbol{D}(e) = \boldsymbol{K}(e) - \boldsymbol{E}(e)$, $\boldsymbol{B}(e) = \boldsymbol{K}(e) - \boldsymbol{D}(e)$, $e^2\boldsymbol{C}(e) = \boldsymbol{D}(e) - \boldsymbol{B}(e)$ and (R_1, R_2) are the principal radii of curvature. The problem is closed adding the equation for the total normal force P

$$P = 2\pi ab\left[p_1 - \frac{1}{3}\left(\alpha a^2 + \beta b^2\right)\right] \tag{9}$$

or for the indentation δ $(= w_{00})$ [29]

$$\delta = \left(\frac{b}{E^*}\right)\left[2p_1\boldsymbol{K} - \alpha a^2\boldsymbol{B} - \beta b^2\boldsymbol{D}\right] \tag{10}$$

which, in the original case of JG, closes the system of 5 equations (5,6,8,9 (or 10)) in the 5 unknowns $(a, b, p_1, \alpha, \beta)$. For $R_1 = R_2$ this corresponds to the classical JKR solution.

III. THE EFFECT OF TANGENTIAL FORCE

A. Theoretical model

Assume that we have a sphere of radius R in adhesive contact with a halfspace (see Fig. 1b).

If a tangential shearing force Q is applied, and no slip occurs in the contact area, a singular shear traction distribution of the form

$$q(x,y) = q_0/\sqrt{1-(x/a)^2-(y/b)^2} \tag{11}$$

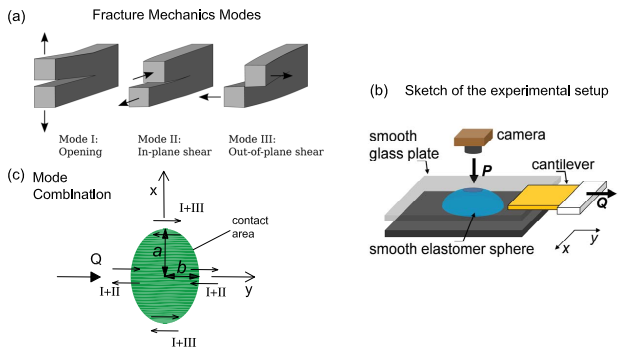

FIG. 1. (a) Fracture mechanics rupture modes (from [30]). (b) Sketch of the experimental setup used in Sahli et al. [15] and in the companion Letter [24]. (c) Combination of the modes along the periphery of the contact patch.

will arise at the interface. Experimental inspection of contact area in this condition shows the contact patch is nearly elliptical and shrinks along the direction of the applied shearing force (mode II), while remaining slightly affected in the perpendicular direction (mode III) (see sketch Fig. 1c, the companion Letter [24], [15], [8] and [19]). A shear traction distribution of the form (11) gives a tangential force $Q = 2\pi abq_0$ and produces at the major axis $K_{II}(a) = 0$ and $K_{III}(a) = q_0\sqrt{\pi a}$, while at the minor axis, $K_{II}(b) = q_0\sqrt{\pi b}$, $K_{III}(b) = 0$. The energy release rate according to standard Fracture Mechanics arguments is $G = \frac{1}{2E^*}\left(K_I^2 + K_{II}^2 + \frac{1}{1-\nu}K_{III}^2\right)$, thus using (5,6) the equivalent SIF at the major "a" and minor "b" axes are

$$K_{eq}(a) = \sqrt{K_I^2(a) + \frac{1}{1-\nu}K_{III}^2(a)} = \sqrt{(\alpha a^2 - p_1)^2 + 2q_0^2}\sqrt{\pi a} \tag{12}$$

$$K_{eq}(b) = \sqrt{K_I^2(b) + K_{II}^2(b)} = \sqrt{(\beta b^2 - p_1)^2 + q_0^2}\sqrt{\pi b} \tag{13}$$

The critical energy needed for the external crack to advance, G_c, depends on the "mode-mixity". Following Hutchinson & Suo [26] we shall postulate that G_c depends on the phase angles $\psi_2 = \arctan\left(\frac{K_{II}}{K_I}\right)$ and $\psi_3 = \arctan\left(\frac{K_{III}}{K_I}\right)$, thus at the minor (where we have modes I and II) and major (where we have modes I and III) axes we write respectively $G_c = G_{Ic}f_{II}(\psi_2)$ and $G_c = G_{Ic}f_{III}(\psi_3)$, i.e.

$$\sqrt{(\beta b^2 - p_1)^2 + q_0^2}\sqrt{\pi b} = K_{Ic}\sqrt{f_{II}(\psi_2)} \tag{14}$$

$$\sqrt{(\alpha a^2 - p_1)^2 + \frac{1}{1-\nu}q_0^2}\sqrt{\pi a} = K_{Ic}\sqrt{f_{III}(\psi_3)} \tag{15}$$

where $f_{II}(\psi_2)$ and $f_{III}(\psi_3)$ are two MMFs which take into account the mixed-mode dependent toughness of the interface.

To sum up, the problem is reduced to a system of 5 equations in the 5 unknown $(a, b, p_1, \alpha, \beta)$[33]

$$\begin{cases} \sqrt{(\beta b^2 - p_1)^2 + q_0^2}\sqrt{\pi b} - \sqrt{2E^*G_{Ic}f_{II}(\psi_2)} = 0 \\ \sqrt{(\alpha a^2 - p_1)^2 + \frac{1}{1-\nu}q_0^2}\sqrt{\pi a} - \sqrt{2E^*G_{Ic}f_{III}(\psi_3)} = 0 \\ \left(\frac{b}{E^*}\right)\left[(\boldsymbol{D}+\boldsymbol{C})\alpha - (b/a)^2\boldsymbol{C}\beta\right] - \frac{1}{2R_1} = 0 \\ \left(\frac{b}{E^*}\right)\left[-\boldsymbol{C}\alpha + \left\{\boldsymbol{B}+(b/a)^2\boldsymbol{C}\right\}\beta\right] - \frac{1}{2R_2} = 0 \\ P - 2\pi ab\left[p_1 - \frac{1}{3}\left(\alpha a^2 + \beta b^2\right)\right] = 0 \end{cases} \tag{16}$$

where, if the punch is axisymmetric[34] $R_1 = R_2 = R$. In principle, if one knows how the interfacial toughness depends on the mode combination, this problem can be solved exactly, with the sole approximation that the equality of the SIFs with their critical values is guaranteed only at the major and minor axes in line with JG approximation.

Next, the following dimensionless notation is introduced [31]

$$\begin{aligned} &\gamma = \sqrt{\frac{R_2}{R_1}}; \qquad R_e = \sqrt{R_2R_1}; \qquad \xi = \left(\frac{E^*R_e}{G_{Ic}}\right)^{1/3}; \\ &\widetilde{a} = \frac{\xi a}{R_e}; \qquad \widetilde{b} = \frac{\xi b}{R_e}; \qquad g = \frac{b}{a}; \qquad \widetilde{\delta} = \frac{\xi^2\delta}{R_e}; \\ &\widetilde{Q} = \frac{Q}{R_eG_{Ic}}; \qquad \widetilde{P} = \frac{P}{R_eG_{Ic}}; \qquad \widetilde{\alpha} = \frac{R_e^2\alpha}{\xi E^*}; \\ &\widetilde{\beta} = \frac{R_e^2\beta}{\xi E^*}; \qquad \widetilde{p}_1 = \frac{\xi p_1}{E^*}; \qquad \widetilde{q}_0 = \frac{\xi q_0}{E^*} \end{aligned} \tag{17}$$

and the system of eq. (16) is written in dimensionless form

$$\begin{cases} \sqrt{\left(\widetilde{\beta}g^2\widetilde{a}^2 - \widetilde{p}_1\right)^2 + \left(\frac{\widetilde{Q}}{2\pi\widetilde{a}^2g}\right)^2}\sqrt{\pi g\widetilde{a}} - \sqrt{2f_{II}(\psi_2)} = 0 \\ \sqrt{(\widetilde{\alpha}\widetilde{a}^2 - \widetilde{p}_1)^2 + \frac{1}{1-\nu}\left(\frac{\widetilde{Q}}{2\pi\widetilde{a}^2g}\right)^2}\sqrt{\pi\widetilde{a}} - \sqrt{2f_{III}(\psi_3)} = 0 \\ \widetilde{a}g\left[(\boldsymbol{D}+\boldsymbol{C})\widetilde{\alpha} - g^2\boldsymbol{C}\widetilde{\beta}\right] - \frac{\gamma}{2} = 0 \\ \widetilde{a}g\left[-\boldsymbol{C}\widetilde{\alpha} + \left\{\boldsymbol{B}+g^2\boldsymbol{C}\right\}\widetilde{\beta}\right] - \frac{1}{2\gamma} = 0 \\ \widetilde{P} - 2\pi g\widetilde{a}^2\left[\widetilde{p}_1 - \frac{\widetilde{a}^2}{3}\left(\widetilde{\alpha} + \widetilde{\beta}g^2\right)\right] = 0 \end{cases} \tag{18}$$

where we used $\widetilde{q}_0 = \frac{\widetilde{Q}}{2\pi\widetilde{a}^2g}$. If, in place of the normal force $\widetilde{P}$, the normal indentation $\widetilde{\delta}$ is controlled, the last equation in (18) is replaced by

$$\widetilde{\delta} = \widetilde{b}\left[2\widetilde{p}_1\boldsymbol{K} - \widetilde{\alpha}\widetilde{a}^2\boldsymbol{B} - \widetilde{\beta}\widetilde{b}^2\boldsymbol{D}\right] \tag{19}$$

For a tangential displacement controlled experiment we recall that an elliptical shear distribution as in (11)

produces a uniform tangential displacement δ_T equal to [32]

$$\delta_T = \frac{Q}{\pi a E^* (1-\nu)} \left[\boldsymbol{K} - \frac{\nu}{1-g^2} (\boldsymbol{K} - \boldsymbol{E}) \right]; \qquad b < a \tag{20}$$

where we used the identity $E^* = \frac{E}{1-\nu^2}$ and $q_0 = \frac{Q}{2\pi a b}$. In dimensionless form $\widetilde{\delta}_T = \delta_T \xi^2 / R$ gives

$$\widetilde{\delta}_T = \frac{\widetilde{Q}}{\pi \widetilde{a} (1-\nu)} \left[\boldsymbol{K} - \frac{\nu}{1-g^2} (\boldsymbol{K} - \boldsymbol{E}) \right]; \qquad \widetilde{b} < \widetilde{a} \tag{21}$$

so that $\widetilde{Q}$ may be replaced by $\widetilde{\delta}_T$ in (18).
Although the theoretical model has been derived with the hypothesis of having the tangential force Q aligned with the minor axis (y direction in Fig. 1b and c), it can be trivially rewritten with Q aligned with the major axis.

B. Mode-mixity function estimation

As shown in Papangelo & Ciavarella [23] for the axisymmetric case, the model results are very sensitive to the exact choice of the phenomenological mode-mixity function. After testing the Literature models available, e.g. the models proposed by Hutchinson & Suo [26], we decided to extract the mode-mixity function from a calibration experiment.

Assume that for a given experimental set-up we know the geometry (R_1, R_2), the applied normal force P (or indentation δ), and for each tangential force Q the corresponding semi-axes of the contact patch (a, b). It is possible to estimate the MMFs $f_{II}(\psi_2)$ and $f_{III}(\psi_3)$ by the following procedure. First, from (18, eq. 3-4) one obtains $\left(\widetilde{\alpha}, \widetilde{\beta}\right)$

$$\widetilde{\alpha} = \frac{\gamma^2 \boldsymbol{B} + \left(1+\gamma^2\right) g^2 \boldsymbol{C}}{2\widetilde{a} g \gamma \left[g^2 \boldsymbol{C}\boldsymbol{D} + \boldsymbol{B} (\boldsymbol{C} + \boldsymbol{D}) \right]} \tag{22}$$

$$\widetilde{\beta} = \frac{\left(1+\gamma^2\right) \boldsymbol{C} + \boldsymbol{D}}{2\widetilde{a} g \gamma \left[g^2 \boldsymbol{C}\boldsymbol{D} + \boldsymbol{B} (\boldsymbol{C} + \boldsymbol{D}) \right]} \tag{23}$$

then, using (18, eq. 5) one computes $\widetilde{p}_1$

$$\widetilde{p}_1 = \frac{\widetilde{P}}{2\pi g \widetilde{a}^2} + \frac{\widetilde{a}^2}{3} \left(\widetilde{\alpha} + \widetilde{\beta} g^2 \right) \tag{24}$$

hence finally from (18, eq. 1-2) one obtains

$$f_{II,\exp}(\psi_2) = \frac{\pi g \widetilde{a}}{2} \left[\left(\widetilde{\beta} g^2 \widetilde{a}^2 - \widetilde{p}_1 \right)^2 + \left(\frac{\widetilde{Q}}{2\pi \widetilde{a}^2 g} \right)^2 \right] \tag{25}$$

$$f_{III,\exp}(\psi_3) = \frac{\pi \widetilde{a}}{2} \left[\left(\widetilde{\alpha} \widetilde{a}^2 - \widetilde{p}_1 \right)^2 + \frac{1}{1-\nu} \left(\frac{\widetilde{Q}}{2\pi \widetilde{a}^2 g} \right)^2 \right] \tag{26}$$

The corresponding phase angles will be for mode I-II interaction

$$\psi_2 = \arctan\left(\frac{K_{II}}{K_I} \right) = \arctan\left(\frac{\widetilde{Q}}{2\pi \widetilde{a}^2 g \left(\widetilde{\beta} \widetilde{a}^2 g^2 - \widetilde{p}_1 \right)} \right) \tag{27}$$

and for mode I-III interaction

$$\psi_3 = \arctan\left(\frac{K_{III}}{K_I} \right) = \arctan\left(\frac{\widetilde{Q}}{2\pi \widetilde{a}^2 g \left(\widetilde{\alpha} \widetilde{a}^2 - \widetilde{p}_1 \right)} \right) \tag{28}$$

IV. COMPARISON WITH EXPERIMENTAL RESULTS

A. Determining the mode-mixity function

Let us consider the experimental data discussed in the companion Letter [24] and in Sahli et al. [15]. The experimental set-up is composed of a cantilever which sustains a glass substrate which is pressed against a PDMS sphere of radius R and then sheared (see Fig. 1c). A camera was used to track the contact area evolution while a force cell simultaneously measured the tangential force applied. The experimental results reported by Sahli et al. [15] and further analyzed in the companion Letter [24] are provided for the following set of normal forces $P = [0.27, 0.55, 0.82, 1.10, 1.37, 1.65, 1.92, 2.12]$ N which span one order of magnitude and for the following sphere radius $R = 9.42$ mm.

To estimate the MMFs the aforementioned procedure was used, i.e. the equations (22,23,24,25,26), for the arbitrarily selected data corresponding to the case $P = 0.55$ N[35]. For the PDMS/glass interfaces we used the following material properties (see [15] and their *Supporting Information*)

$$\begin{gathered} G_{Ic} = 27 \text{ mJ/m}^2; \qquad E = 1.88 \text{ MPa}; \\ \nu = 0.5; \qquad \sigma = 0.41 \text{ MPa}; \end{gathered} \tag{29}$$

where σ is the best fitted average shear strength of the interface (see Fig. 4) and E was obtained from the control experiment[36] with $P = 0.55$ N. Figure (2a) shows

the experimental data (orange triangles) and the interpolated (black solid line) MMF $f_{II}(\psi_2)$ as a function of the phase angle ψ_2. $f_{II}(\psi_2)$ can be well approximated by $\log[f_{II}(\psi_2)] = a_2\psi_2^2 + b_2\psi_2^{n_2}$, where the coefficients are $(a_2, b_2, n_2) = \left(1.18, 5.67 * 10^{-2}, 7.05\right)$. To obtain a better fit, the data were interpolated in log-linear form, i.e. $(\psi_2, \log[f_{II}(\psi_2)])$, which allows to catch the MMF across all scales. The inset shows the interpolated mode-II MMF versus the one evaluated from all the set of experimental data available, which do collapse over 3 orders of magnitude of f_{II}. With the same procedure, $f_{III}(\psi_3)$ has been interpolated from the experimental data using solely the set of data corresponding to the case $P = 0.55$ N (Fig. 2b). $f_{III}(\psi_3)$ can be well approximated by $\log[f_{III}(\psi_3)] = a_3\psi_3^2 + b_3\psi_3^{n_3}$, where the coefficients are $(a_3, b_3, n_3) = \left(1.87, 6.73 * 10^{-3}, 15.20\right)$. The inset shows that the complete set of experimental data align along the main diagonal, nevertheless the data referring to the higher normal forces, i.e. $P \approx [1.65, 1.92, 2.12]$ N, appear to be shifted by a factor ≈ 2 also for vanishing tangential forces $(f(\psi) \simeq 1)$, which indicates a small deviation in the original JKR fit (see the 3 rightmost points in Fig. 3). It is worth noting that the normal force is varying by one order of magnitude in the same set of experiments, hence some nonlinear effects (probably due to stiffening in the material) may have arisen which make the JKR fit not perfect. Figure 3 shows the JKR curve (black solid line) obtained with the parameters reported in the companion Letter [24] and by Sahli et al. [15] (see (29)) and for each normal force the contact area under null shear force (red dots). It can be observed that the deviations from JKR are very small.

B. Decay of contact area

In this section the results obtained solving the system of equations (18) are presented, where the unknown MMFs $f_{II}(\psi_2)$ and $f_{III}(\psi_3)$ have been substituted by the one estimated in the previous section using only the data set for $P = 0.55$ N. Fig. 4 shows the contact area evolution as a function of the tangential force for the complete set of experimental data from Sahli et al. [15] with $R_e = R = 9.42$ mm (PDMS sphere/glass substrate contact). The markers indicate the experimental results obtained for each normal force, while the black solid lines are for the proposed model, that proves to be in very good agreement with all the observations. Small deviations appear for the heavier normal forces as was already found and discussed in the previous section. The dashed red line shows the full sliding threshold according to the criterion $Q_s = \sigma * A$, as proposed by Sahli et al. [15] and Mergel et al. [8]. Figure 5 favorably compares the mean shear stress at the interface $\overline{\sigma} = Q/A$ according to the experimental results (markers) and to the proposed model (solid black lines), where the red dashed lines marks the boundary of the full sliding region, i.e. $\overline{\sigma} = \sigma = 0.41$ MPa.

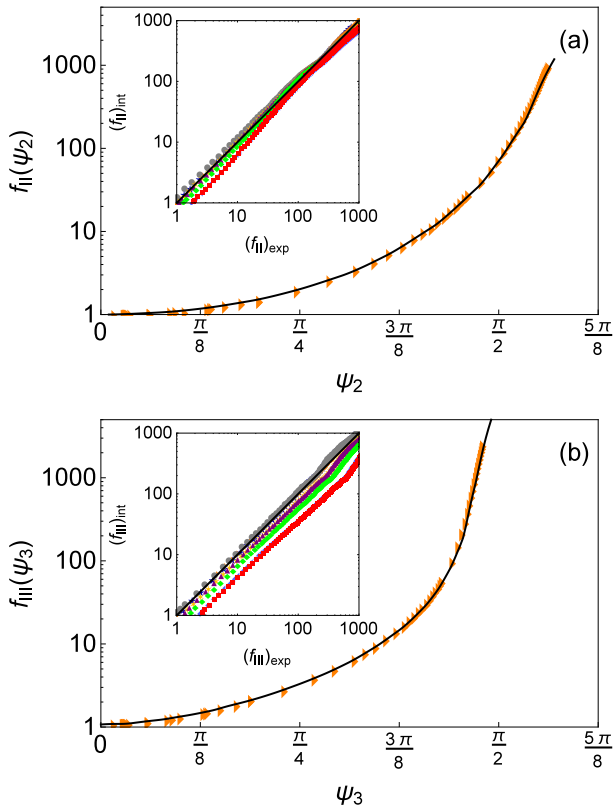

FIG. 2. Orange triangles: mode-mixity functions (a) $f_{II}(\psi_2)$ (respectively (b) $f_{III}(\psi_3)$) estimated from eq. (25) (respectively (26)) from the experimental data of case $P = 0.55$ N. Solid lines: interpolation of the curves used in the comparison with other experimental data available in the companion Letter [24]. Insets: interpolated vs experimental MMFs for all experiments. Solid lines: equality lines. Markers for experimental results. Blue stars, orange right-triangles, gray circles, yellow stars, purple up-triangles, green diamonds, violet left-triangles, red squares respectively for $P = [0.27, 0.55, 0.82, 1.10, 1.37, 1.65, 1.92, 2.12]$ N.

V. CONTACT SHEARING ALONG THE MAJOR/MINOR SEMI-AXES

Let us compare the model predictions with the experimental results in terms of evolution of the ellipticity (or flattening) $F = 1 - b/a$. For this comparison, the set of experimental data for $P = 1.10$ N and $R_e = R = 9.42$ mm has been chosen. In Fig. 6a the ellipticity is plotted against the tangential force Q: the experimental data are plotted with orange stars, while the model prediction is shown as a black solid line. The same set of data is plotted in Fig. 6b in terms of evolution of the semi-axes (a, b). Notice that the contact area shrinks drastically along the direction aligned with the tangential force, semi-axis "b", while the perpendicular axis "a" remains mostly unaffected by the tangential force. This is in agreement with

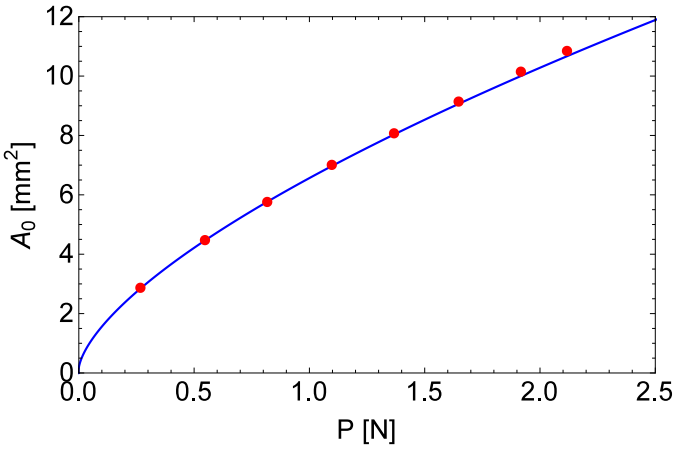

FIG. 3. Contact area under null tangential force A_0 vs normal force P. Solid line: JKR model with $G_{Ic} = 27$ mJ/m^2, $E = 1.88$ MPa, $\nu = 0.5$ and $R = 9.42$ mm. Red dots: experimental data under null tangential force.

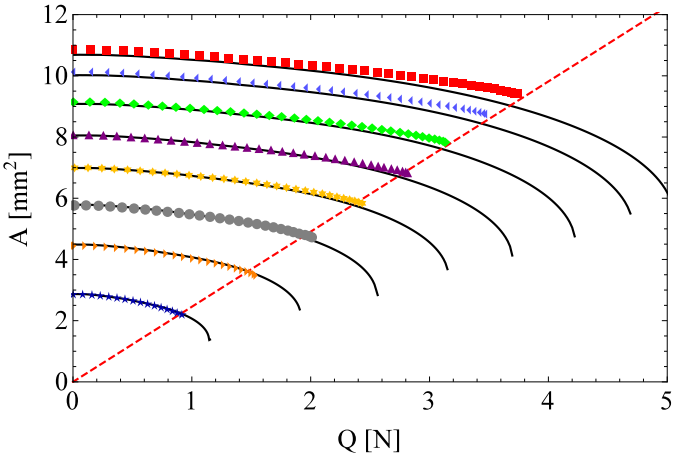

FIG. 4. Contact area A as a function of the tangential force Q for different normal forces $P = [0.27, 0.55, 0.82, 1.10, 1.37, 1.65, 1.92, 2.12]$ N and $R_e = R = 9.42$ mm. The markers indicate the experimental measurements, the solid black lines show the model prediction while the dashed red line indicates the full sliding criterion $Q_s = \sigma * A$ with $\sigma = 0.41$ MPa.

the observation that the interfacial toughness under the mode combination I-III was found greater than under mode I-II combination (compare $f_{II}(\psi_2)$ and $f_{III}(\psi_3)$ in Fig. 2). The predictions are in excellent agreement with the experimental results of [24].

We then investigated the indentation of a non-axisymmetric punch with $R_e = R = 9.42$ mm and $R_2/R_1 = 1/2$, so as in the typical rough contacts according to Greenwood [25], being all the other parameters unchanged. For the latter case no experimental data are available to compare with, thus only the model predictions are presented. Figure 6a shows the evolution of

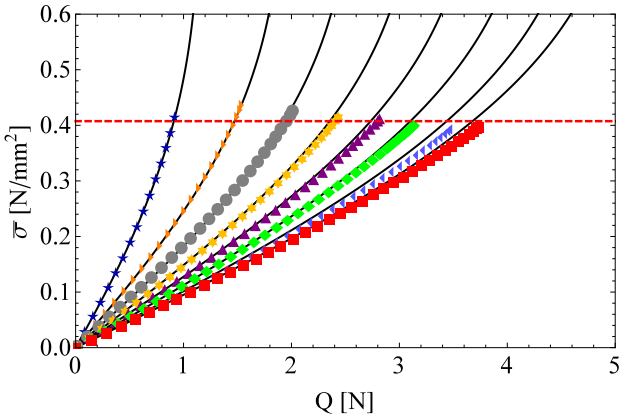

FIG. 5. Mean shear stress at the interface $\overline{\sigma} = Q/A$ according to the experimental results from Sahli et al. [15] (markers) and to the proposed model (solid black lines). The solid lines are drawn for $P = [0.27, 0.55, 0.82, 1.10, 1.37, 1.65, 1.92, 2.12]\,N$ and $R_e = R = 9.42$ mm. The red dashed line marks the full sliding points at $\overline{\sigma} = \sigma = 0.41$ MPa.

the ellipticity when the punch is loaded along its major (red dashed line) and minor (blue dotdashed line) axis. The same results are plotted in terms of semi-axes evolution in Fig. 6b. Notice that after shearing, the contact patch shapes are strongly different among the three cases we have analyzed, i.e. axisymmetric punch, and non-axisymmetric punch loaded along the major or minor axis. Indeed the axis under mode II loading tends to shrinks much more rapidly with respect to the axis under mode III loading. Hence the punch loaded along its major axis shrinks towards a more circular shape, i.e. the ellipticity decreases, and eventually becomes negative as due to the shearing force, we obtain $a < b$. On the contrary, loading along the minor axis produces a contact patch with increasing ellipticity while Q is increased.

The theoretical model is based on the assumption that the contact area shrinks in an elliptical fashion while the contact is sheared. In Fig. 7 we check this assumption comparing with actual experimental snapshots of the contact area (same data used for Fig. 6) taken for 5 tangential forces, from Q_1 to Q_5 respectively $[0.04, 0.77, 1.42, 1.98, 2.38]$ N. The results are reported for $R_e = R$ and respectively $R_2/R_1 = 1$ (middle row) and $R_2/R_1 = 1/2$ (top and bottom row) where the shearing force is aligned with the minor (top row) and major (bottom row) axis. The evolution of the contact patches according to the proposed model is shown as a red dashed line (all rows) while the experimental contact patches are plotted as a black patch (middle row). The agreement between experimental results and model prediction is excellent for the axisymmetric punch, while we can provide only predictions for $R_2/R_1 = 1/2$ as experimental data are missing.

Finally, we further explore the effect of the initial ge-

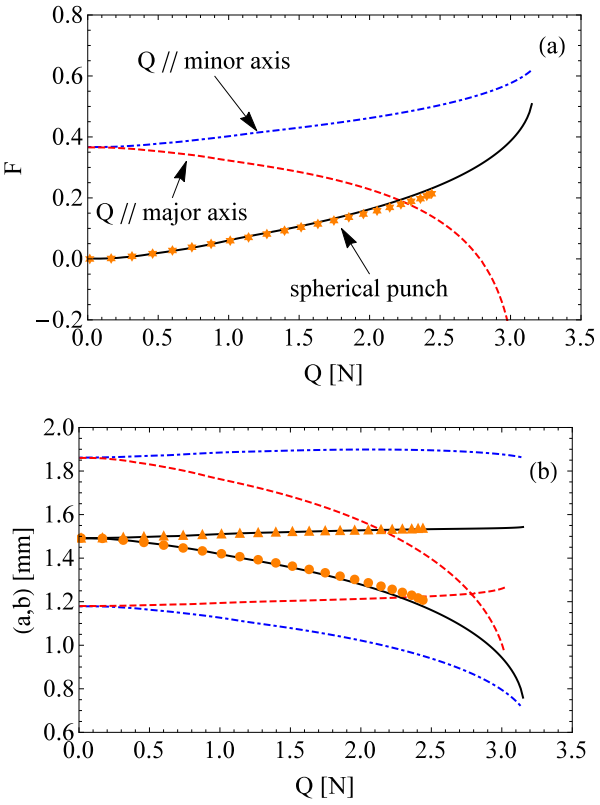

FIG. 6. (a) Ellipticity $F = 1 - b/a$ versus the tangential force Q as obtained experimentally for $P = 1.10$ N, $R_e = R = 9.42$ mm (orange stars) and as obtained from the model (solid black line). Prediction of the ellipticity evolution for a non-axisymmetric punch with $R_2/R_1 = 1/2$ ($R_e = 9.42$ mm) loaded along its major (dashed red line) or minor (blue dotdashed line) axis. (b) Evolution of the the semi-axes (a, b), with $a > b$ at $Q = 0$ N. Symbols and lines as in panel (a).

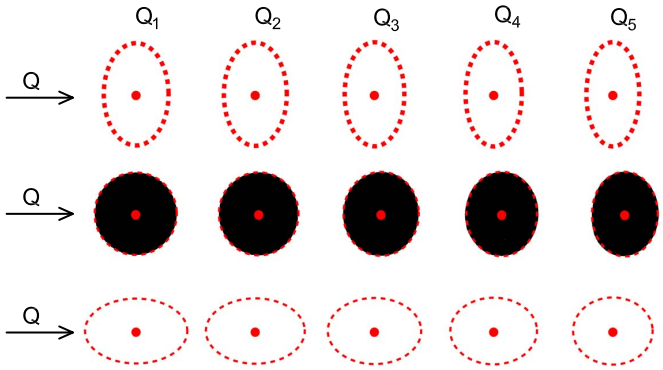

FIG. 7. Evolution of the contact patches according to the proposed model (red dashed line) for: $R_2/R_1 = 1/2, R_e = R$ loaded respectively along the minor (top row) and major (bottom row) axis and for $R_1 = R_2 = R$ (middle row). For the axisymmetric case (middle row) experimental contact patches are plotted in black. The tangential forces range from Q_1 to Q_5, respectively $[0.04, 0.77, 1.42, 1.98, 2.38]$ N. For all the snapshots $P = 1.10$ N.

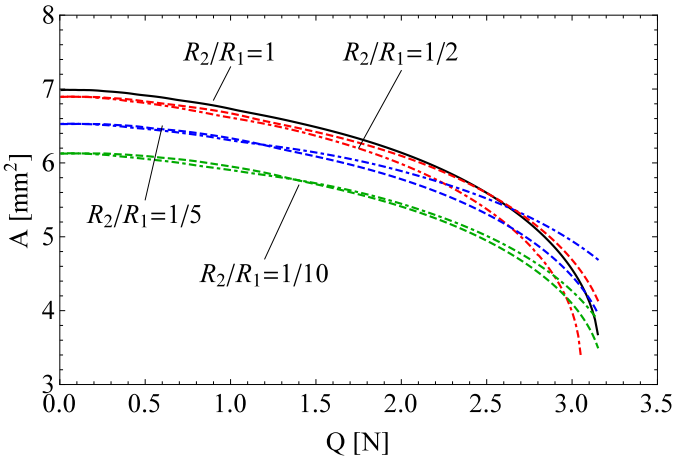

FIG. 8. Evolution of the contact area with the tangential force reported for $R_e = R = 9.42$ mm, $P = 1.10$ N, $R_2/R_1 = [1, 1/2, 1/5, 1/10]$ respectively solid black line, red, blue and green lines. Predictions have been made for both Q aligned with the major (dotdashed lines) and minor (dashed lines) axis.

ometry, R_2/R_1 ratio, on the contact area decay. In Fig. 8 the evolution of contact area with the tangential force is reported for $R_e = R = 9.42$ mm, $P = 1.10$ N, $R_2/R_1 = [1, 1/2, 1/5, 1/10]$ respectively solid black line, red, blue and green lines. Predictions have been made for both Q aligned with the major (dotdashed lines) and minor (dashed lines) axis. One concludes that the contact shapes are affected by both the punch geometry and the direction of shear with respect to the ellipse orientation. Inspection of Fig. 8 reveals that in terms of overall contact area decay for increasing shear force Q, changing the ratio R_2/R_1 from 1 to 1/10 will produce a reduction of the overall contact area of the order of $10 - 15\%$ for both Q aligned along the major (dotdashed line) or minor (dashed) axis.

VI. SCALING LAW FOR AREA DECAY

In their paper, Sahli et al [15] showed that for smooth spheres a quadratic form $A(Q) = A_0 - \alpha_A Q^2$ well captures the decay of contact area with tangential force, where A_0 is the contact area for $Q = 0$ N and α_A is a fitting coefficient. Interestingly, they found that α_A shows a power law scaling with A_0 with exponent $-3/2$ over 4 orders of magnitude which comprises data from interfacial microjunctions (rough contacts) and data from smooth spheres. Literature LEFM axisymmetric models

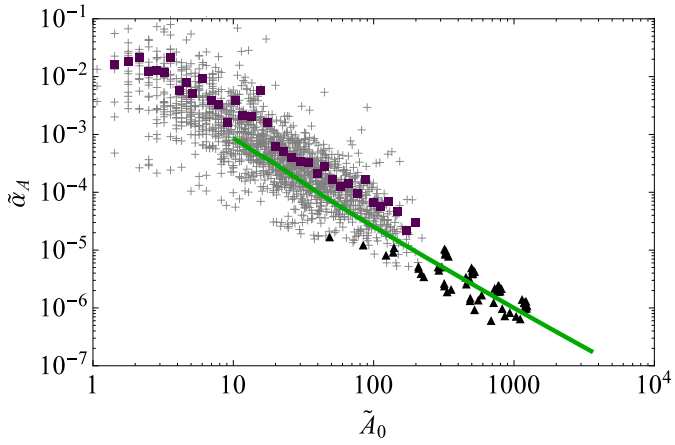

FIG. 9. Greeen solid line: coefficient $\widetilde{\alpha}_A$ obtained fitting the numerical data obtained by the proposed elliptical model with a power law function $\widetilde{A}(Q) = \widetilde{A}_0 - \widetilde{\alpha}_A \widetilde{Q}^2$ as proposed by Sahli et al. [15] as a function of $\widetilde{A_0}$. Symbols represent the experimental data reported in [15]: triangles for smooth sphere with radii $R = [7.06, 9.42, 24.81]$ mm, crosses refer to the experimental data obtained for microjunctions (rough contact) with average values indicated by purple squares.

for smooth spheres ([22], [23]) have found a similar but not equal exponent, i.e. $-5/4$.

Here we investigate which scaling law would arise from the present elliptical model and compare with experimental results. We defined a set of normal forces ranging from 1 mN to 10 N and, using the model, obtained the area vs tangential force curves up to full sliding, i.e. truncating them at $Q_s = \sigma * A$. We used the same material properties (29) and geometry parameters $R_e = R = 9.42$ mm adopted in the previous analyses. The resulting curves were fitted with a quadratic area decay law that in dimensionless form reads $\widetilde{A}(\widetilde{Q}) = \widetilde{A}_0 - \widetilde{\alpha}_A \widetilde{Q}^2$, being $\widetilde{A} = A(\xi/R_e)^2$ and $\widetilde{\alpha}_A = \alpha_A \left(\xi G_{Ic}\right)^2$. To this end we needed to estimate the mean microjunction radius. We consider the results of a single rough contact experiment from Ref. [15]:, PDMS/glass contact, under a normal force of $P = 6.40$ N for which 514 microcontacts with an initial area larger than $2{*}10^{-9}$ m^2 were found and tracked. This results in an average force for each microjunction equal to $P_i = 6.4/514 \simeq 1.2 \times 10^{-2}$ N. From the distribution of microjunctions contact areas we derived the characteristic dimension of the microjunction $a_i = \sqrt{A_i/\pi}$ and computed the mean contact radius $\overline{a}_i = 0.235$ mm. Using the JKR model with known P_i, a_i and material properties $G_{Ic} = 27$ mJ/m^2, $E = 1.88$ MPa, $\nu = 0.5$ we estimated the mean radius of curvature $R_{micro} \approx 2.6$ mm. In Fig. 9,$\widetilde{\alpha}_A$ is shown as a function of $\widetilde{A}_0$ (green solid line), with superimposed the experimental data obtained for smooth spheres (black triangles) and microjunctions (raw data: gray crosses, averaged data: purple squares). The agreement between the model and the experimental results is very good over more than 2 orders of magnitude in $\widetilde{A}_0$, but cannot be assessed in the range $1 < \widetilde{A}_0 < 10$. Indeed JKR theory predicts, under force control, that the smallest stable contact spot is $\widetilde{A}_{min,JKR} = \pi(\frac{9\pi}{8})^{2/3} \simeq 7.3$.

Discrepancies may arise at too small contact areas as the decay law may not be strictly quadratic anymore as indeed recent investigations seem to suggest [8, 23]. We reconsidered the obtained area-force curves and fitted them using a power law function with form $A(Q) = A_0 - c_1 Q^n$, from which the best fit exponent n has been obtained. Figure 10a shows the quantity $1 - A(Q)/A_0$ as a function of Q in a log-log plot. The red dots represent the points obtained using the elliptical model while the black solid lines are the best fitted power law functions obtained varying the normal force P over 4 orders of magnitude. One easily recognizes that the lighter the normal force the steeper gets the power law function suggesting that a unique exponent is unlikely to best fit all the curves. In Fig. 10b n is reported as a function of the normal force P (solid curve). The shaded areas indicate the range of normal forces used in the experiments by Sahli et al. [15] and Mergel et al. [8]. Inspection of the graph reveals that for the experiments by Sahli et al. [15] normal forces are of the order of 1 N and the contact area decay in the model is well fitted by a quadratic power law ($n \approx 1.8 - 1.9$), while for lighter normal forces of the order of $10^{-3} - 10^{-2}$ N, as in [8], a larger exponent is found $n \approx 3 \pm 0.5$.

VII. CONCLUSIONS

We have introduced the first non-axisymmetric model which successfully predicts the anisotropic shearing of the contact area under adhesive conditions due to tangential force. The model has been validated against several experimental data from Sahli et al. [15] and included in the companion Letter [24] and essentially an excellent agreement is found. The model is based on LEFM and has been inspired by the seminal work of JG, which has been extended to accomplish tangential loading of the contact area. Using our elliptical model we have made predictions of contact area evolution for non-axisymmetric punches. The results show that the effect of differing principal radii of curvature strongly affects the evolution of the contact shape. This may reveal to be a fundamental phenomenon in the development of contact patch anisotropy in rough contact under shear, where asperities are expected to be mildly elliptical [25]. We have also shown that in terms of overall variation of contact area a reduction of $10 - 15\%$ can be expected varying R_2/R_1 from 1 to 1/10. Deviations from this behaviour may be expected due to the interactions between asperities, but this is out of the scope of the present paper.

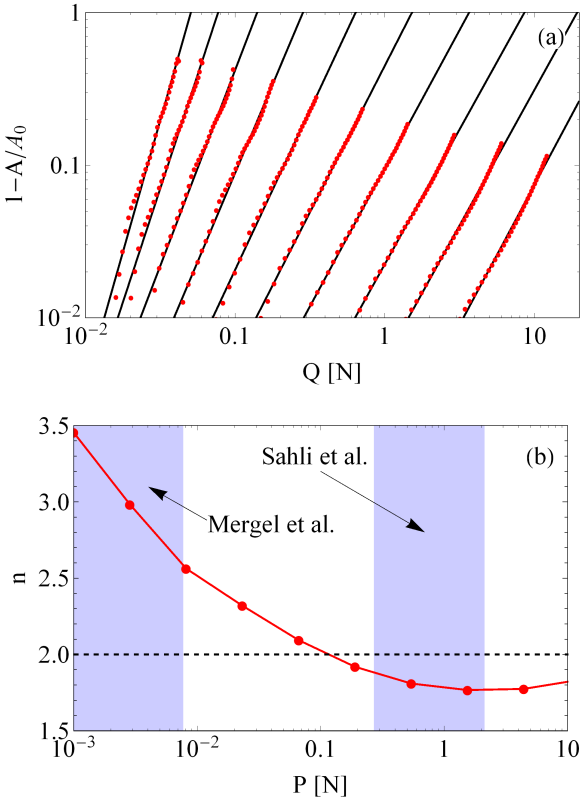

FIG. 10. (a) Best fit of the form $1-A(Q)/A_0 \propto Q^n$ applied to the numerical data obtained by the proposed elliptical model for a range of normal forces ranging from 1 mN to 10 N. Red dots represent the numerical data, while the solid black lines stand for the best fitted power law. The exponent n is reported in panel (b) as a function of the normal force. Shaded areas indicate the regions where Sahli et al. [15] and Mergel et al. [8] data lie.

ACKNOWLEDGEMENTS

A.P. is thankful to the DFG (German Research Foundation) for funding the project PA 3303/1-1. M.C. is supported by the Italian Ministry of Education, University and Research (MIUR) under the Departments of Excellence grant L.232/2016. This work was supported by LABEX MANUTECH-SISE (ANR-10-LABX-0075) of Université de Lyon, within the program Investissements d'Avenir (ANR-11-IDEX-0007) operated by the French National Research Agency (ANR). It received funding from the People Program (Marie Curie Actions) of the European Union's Seventh Framework Program (FP7/2007-2013) under Research Executive Agency Grant Agreement PCIG-GA-2011-303871. We are indebted to Institut Carnot Ingénierie@Lyon for support and funding.

AUTHOR CONTRIBUTION STATEMENT

A.P. and M.C. conceived the theoretical model and wrote the work. A.P. created the figures. J.S., R.S and G.P. provided the experimental data. All the authors revised the work up to its final form.

[1] A.I. Vakis, V.A. Yastrebov, J. Scheibert, L. Nicola, D. Dini, C. Minfray, A. Almqvist, M. Paggi, S. Lee, G. Limbert, J.F. Molinari, G. Anciaux, R. Aghababaei, S. Echeverri Restrepo, A. Papangelo, A. Cammarata, P. Nicolini, C. Putignano, G. Carbone, S. Stupkiewicz, J. Lengiewicz, G. Costagliola, F. Bosia, R. Guarino, N.M. Pugno, M.H. Müser, M. Ciavarella, (2018). Modeling and simulation in tribology across scales: An overview. Tribology International, 125, 169 (2018).

[2] K. Autumn, A. Dittmore, D. Santos, M. Spenko, & M. Cutkosky, (2006), Frictional adhesion: a new angle on gecko attachment. Journal of Experimental Biology, 209(18), 3569-3579.

[3] D. Labonte, & W. Federle, (2016), Biomechanics of shear-sensitive adhesion in climbing animals: peeling, pre-tension and sliding-induced changes in interface strength. Journal of The Royal Society Interface, 13(122), 20160373.

[4] N. Gravish, M. Wilkinson, & K. Autumn, (2008), Frictional and elastic energy in gecko adhesive detachment. Journal of The Royal Society Interface, 5(20), 339-348.

[5] K. L. Johnson, K. Kendall & A. D. Roberts, (1971), Surface energy and the contact of elastic solids. Proc. R. Soc. Lond. A 324, 301–313.

[6] A.M. Homola, J.N. Israelachvili, P.M. McGuiggan, M.L. Gee, (1990), Fundamental experimental studies in tribology: the transition from "interfacial"friction of undamaged molecularly smooth surfaces to "normal"friction with wear. Wear 136 (1), 65–83 .

[7] H. Yoshizawa, Y.L. Chen, J.N. Israelachvili, (1993), Fundamental mechanisms of interfacial friction. 1. Relation between adhesion and friction. J. Phys. Chem. 97 (16), 4128–4140.

[8] J.C. Mergel, R. Sahli, J. Scheibert, R.A. Sauer, (2018), Continuum contact models for coupled adhesion and friction. J. Adhes. (in press) doi:10.1080/00218464.2018.1479258.

[9] E. Rabinowicz, (1961), Influence of surface energy on friction and wear phenomena. Journal of Applied Physics, 32(8), 1440-1444.

[10] E. Rabinowicz, (1992), Friction coefficients of noble metals over a range of loads. Wear, 159(1), 89-94.

[11] Svetlizky, I., & Fineberg, J., (2014), Classical shear cracks drive the onset of dry frictional motion. Nature, 509(7499), 205

[12] Papangelo, A., & Ciavarella, M., (2015), Cattaneo–Mindlin plane problem with Griffith friction. Wear, 342, 398-407.

[13] Papangelo, A., Ciavarella, M., & Barber, J. R., (2015), Fracture mechanics implications for apparent static friction coefficient in contact problems involving slip-weakening laws. Proc. R. Soc. A, 471(2180), 20150271.

[14] Savkoor, A. R. & Briggs, G. A. D., (1977), The effect of a tangential force on the contact of elastic solids in adhesion. Proc. R. Soc. Lond. A 356, 103–114.

[15] R. Sahli, G. Pallares, C. Ducottet, I. E. Ben Ali, S. Al Akhrass, M. Guibert, J. Scheibert, (2018), Evolution of real contact area under shear and the value of static friction of soft materials, Proceedings of the National Academy of Sciences of the USA, 115 (3) 471-476.

[16] Hutchinson, J. W., (1990), Mixed mode fracture mechanics of interfaces. Metal-ceramic interfaces, 4, 295-306.

[17] Johnson KL, (1996), Continuum mechanics modeling of adhesion and friction. Langmuir 12:4510–4513.

[18] Johnson, K. L., (1997), Adhesion and friction between a smooth elastic spherical asperity and a plane surface. In Proceedings of the Royal Society of London A 453, No. 1956, 163-179.

[19] Waters JF, Guduru PR, (2010), Mode-mixity-dependent adhesive contact of a sphere on a plane surface. Proc R Soc A 466:1303–1325.

[20] Popov, V. L. & Dimaki, A. V., (2017), Friction in an adhesive tangential contact in the Coulomb-Dugdale approximation, The Journal of Adhesion, 93:14, 1131-1145

[21] Filippov, A., Popov, V. L., & Gorb, S. N., (2011), Shear induced adhesion: contact mechanics of biological spatula-like attachment devices. Journal of Theoretical Biology, 276(1), 126-131.

[22] Ciavarella, M., (2018), Fracture mechanics simple calculations to explain small reduction of the real contact area under shear. Facta Universitatis, Series: Mechanical Engineering, 16(1), 87-91.

[23] Papangelo, A., & Ciavarella, M., (2019), On mixed-mode fracture mechanics models for contact area reduction under shear load in soft materials. Journal of the Mechanics and Physics of Solids, 124, 159-171.

[24] Sahli R., Pallares G., Papangelo A., Ciavarella M., Ducottet C., Ponthus N., Scheibert J., (2019), Shear-induced anisotropy in rough elastomer contact. Physical Review Letters, 122, 214301.

[25] Greenwood, J. A., (2006), A simplified elliptic model of rough surface contact. Wear, 261(2), 191-200.

[26] Hutchinson, J. W. & Suo, Z., (1992), Mixed mode cracking in layered materials. In Advances in applied mechanics, vol. 29 (eds J. W. Hutchinson & T. Y. Wu), pp. 63–191. Boston, MA: Academic Press.

[27] Johnson, K. L., & Greenwood, J. A., (2005), An approximate JKR theory for elliptical contacts. Journal of Physics D: Applied Physics, 38(7), 1042.

[28] Galin, L.A., Contact Problems (Springer, Netherlands, 2008)

[29] Kalker J J, (1967), On the rolling contact of two elastic bodies in the presence of dry friction PhD Dissertation Delft University of Technology, NL

[30] https://commons.wikimedia.org/wiki/File:Fracture_modes_v2.svg

[31] Maugis D., (2000), Contact, Adhesion and Rupture of Elastic Solids, Springer, New York.

[32] Johnson, K.L.,Contact Mechanics, (1985),Cambridge University Press,Cambridge.

[33] The last equation for the force can be replaced by the respective for indentation (10).

[34] In deriving the model we start with the case of a sheared spherical punch. Nevertheless the model can be also used for non-axisymmetric Hertzian geometry provided that the tangential force is aligned with the minor or major axis.

[35] Similar results can be obtained selecting the set of data corresponding to a different normal force.

[36] For the control experiment with $P = 0.55$ N, under zero tangential force, a contact area $A_0 \simeq 4.48$ mm^2 was measured. Using the JKR relation $P = \frac{4E^*}{3R}\left(\frac{A_0}{\pi}\right)^{3/2} - \sqrt{8\pi^{-1/2}{E^*}{A_0}^{3/2}G_{Ic}}$ with $G_{Ic} = 27$ mJ/m^2, $\nu = 0.5$ and $R = 9.42$ mm one gets $E \simeq 1.88$ MPa.